Investigating the photoactivity of Cu_2O-TiO_2 (Home Prepared) composites for H_2 production by photoreforming under natural solar light in a pilot plant photoreactor

Muhammad Umair[1], Alba Ruiz-Aguirre[2], Ilaria Berruti[2], Leonardo Palmisano[1], Sixto Malato Rodríguez[2,*], Vittorio Loddo[1], Marianna Bellardita[1,*]

[1]Engineering Department, University of Palermo, Viale delle Scienze Ed. 6, Palermo 90128, Italy.
[2]CIEMAT – Plataforma Solar de Almería, Ctra. De Senés s/n, Tabernas, 04200 Almería, Spain

[*] Corresponding authors:
Marianna Bellardita (E-mail: marianna.bellardita@unipa.it)
Sixto Malato Rodríguez (E-mail: smalato@psa.es)

Abstract

Home-prepared TiO_2 containing an anatase/rutile mixture was coupled with different Cu_2O amounts by the ball method technique. The samples were characterized by UV-Vis diffuse spectroscopy (DRS), specific surface area (SSA) determination, photoluminescence (PL) and Raman spectra, X-ray diffraction (XRD), scanning electron microscopy (SEM), transmission electron microscopy (TEM), and X-ray photoelectron spectroscopy (XPS), Electron Paramagnetic Resonance (EPR) and photoelectrochemical measurements. The photocatalytic activity was studied for H_2 production under natural solar light irradiation in a pilot plant reactor in the presence of different sacrificial agents. An effective heterojunction that enhanced the charge transfer processes, was formed between the components, as confirmed by photoluminescence spectra. 3%Cu_2O-TiO_2 was the most active photocatalyst and the presence of Cu_2O (instead of the noble metals generally used) was efficient for H_2 production with 62 mmol obtained after 5h (equivalent to ca. 5 mmol g^{-1} h^{-1}) of solar irradiation starting from glycerol, which yielded the highest H_2

amount with respect to the other sacrificial agents. Copper was present in different oxidation states and a certain amount of leaching of Cu species was observed. Holes, $OH^{\bullet}$ and $O_2^{\bullet-}$ radicals were the main active species for glycerol degradation, while a higher availability of photoproduced electrons was beneficial for H_2 production.

Keywords: photocatalysis; semiconductor composites; glucose; ethanol; glycerol; solar photo-reactor.

1. Introduction

Population growth and industrialization have resulted in an immense increase in energy demand worldwide. To meet these energy needs, fossil fuels such as coal, natural gas, and gasoline have been the main energy resources, however, their use is no longer feasible due to the restrictions to the emissions of CO_2 and other greenhouse gases (GHG) responsible for global warming [1-3]. Thus, there is a need to develop environmentally sustainable options for the energy supply to achieve carbon neutrality, included in the European Green Deal (EGD) [4]. Hydrogen gas (H_2) can be considered a clean energy fuel, producing only water when reacts with O_2, and displaying a higher energy density (122 $kJ \cdot g^{-1}$) than traditional fuels [5]. Conventional industrial methods used for H_2 production require high temperatures (700-1100 ^{o}C) and cause large amounts of GHG emissions [6]. Thus, there is an urgent need to find green alternative methods. Solar energy is a natural, powerful, renewable, and cost-free energy source and with a suitable technology can be converted to chemical fuel [7]. The photoreforming of organic compounds is a promising and sustainable method utilizing sunlight and semiconductors for H_2 production [8]. In particular,

biomass derivatives are considered renewable because they are formed naturally from plants by photosynthesis and have zero greenhouse effect [9]. The most common organic compounds used for H_2 production are alcohols, such as glycerol, ethanol and methanol, as well as formic acid and sugars. Ethanol, which is produced from low-grade biomass and sewage sludge, provides a sustainable and economical route to produce H_2 through its photoreforming [10]. Formic acid is a cheap, non-flammable, non-toxic and highly stable compound, whose formula is 4.4% (w/w) hydrogen and is considered very suitable because it decomposes directly into H_2 and CO_2 by a thermodynamically favourable reaction [11, 12]. Another interesting candidate is glucose, which is obtained from cellulose and starch, and can be used for the production of high-value chemicals and H_2 fuel [13, 14]. The use of glycerol is particularly attractive because it accounts for ~10 % of the volume of the biodiesel industries [15] and with increased biodiesel production, disposal of crude oil is rising as a new issue [16]. The photocatalytic technology represents a promising green method to convert crude glycerol into H_2 that can be used as renewable energy fuel or being converted into valuable chemicals [17, 18].

Although TiO_2 is the most investigated photocatalyst [19] since it was first used as an electrode in 1972 for H_2 production by water-splitting [20], it has many weaknesses to overcome [21]. Various strategies aimed at enhancing the visible light absorption, increasing the surface area, and improving the charge transfer processes, have been investigated to improve the performance of TiO_2 [22-24], with particular attention to H_2 production [25]. Loading TiO_2 surface with noble metals including Pt, Ru, Au, and Pd is very effective in increasing photocatalytic H_2 production [26, 27], enhancing the separation of photogenerated charges through Schottky barrier formation, inducing surface plasmon resonance (SPR), generation of gap states by interaction with TiO_2 VB states. However, for practical applications this option is limited due to the high cost of noble

71 metals. Combining TiO_2 with another semiconductor to form a heterojunction is a successful
72 strategy to inhibits the hole–electron pairs recombination [28, 29]; notably, choosing
73 semiconductors with appropriate conduction and valence band energy levels, H^+ reduction to H_2
74 is thermodynamically favourable [30-32].
75 TiO_2 exists in three main polymorphs, i.e. anatase, brookite, and rutile, displaying different energy
76 levels of their valence and conduction bands [33]. It has been demonstrated that the simultaneous
77 presence of multiple TiO_2 phases allows the formation of a heterojunction that has the same
78 behaviour as that formed by coupling different semiconductors [33-35]. This is one of the features
79 that explains the high photocatalytic activity of Degussa P25, the most widely used commercial
80 TiO_2 [36, 37]. It should be remembered, however, that in addition to the phase composition of
81 TiO_2-based photocatalysts, many other parameters such as the presence of defects, the degree of
82 surface hydroxylation and acidity and basicity, influence their photoactivity [38]. For this reason,
83 there is a continuous effort by researchers in the preparation of photocatalysts with tailored
84 synthesis conditions.
85 As an alternative to noble metals, Cu_2O is a p-type semiconductor with a narrow band gap (2.0-
86 2.2 eV), low cost, low toxicity, and suitable bands energy levels, which, coupled with TiO_2, has
87 proven to be effective in producing H_2 via photoreforming [39,40]. Plascencia-Hernández et al.
88 [39] prepared Cu_xO/TiO_2 (P25) composites via chemical reduction using different amounts of
89 copper chloride. Characterization techniques revealed that, during the photocatalytic reforming of
90 methanol under simulated solar light, Cu was present in different forms (CuO, Cu_2O, and Cu^0).
91 The best results were obtained by loading small amounts of Cu_xO (0.05%w) on TiO_2, affording an
92 H_2 evolution rate of 2.86 mmol g^{-1} h^{-1}. The coexistence of the Cu species and TiO_2 facilitated the
93 effective separation of photogenerated charges, endorsing the photoreduction of protons.

Rajendran et al. [41] tested Cu_xO/TiO_2 photocatalysts with Cu in +1 and/or +2 oxidation state for H_2 generation under sunlight irradiation using a 25% v/v methanol/water mixture. Samples in which Cu is exclusively present in +1 oxidation state exhibited the highest H_2 production rate of 7.06 mmol h^{-1} g^{-1}. A p-n type heterojunction formed at the interface of Cu_2O-TiO_2 improved charge carrier separation and absorbance in the visible spectrum leading to high photocatalytic activity for glycerol photoreforming with an H_2 production of about 4.7 mmol g^{-1} in 24h of irradiation with a 400W metal halide lamp [42]. Cu_2O/TiO_2 (P25) composites obtained by a hydrothermal method showed good activity for H_2 production (evolution rate 2.55 mmol g^{-1} h^{-1}) from aqueous methanol solution under simulated sunlight irradiation in lab-scale reactors [43].

For the preparation of Cu_2O-TiO_2, to date different strategies have been used, but each is associated with some limitations, such as high reagent cost, and high operating temperature and pressure conditions. Ball milling is a simple, inexpensive, reproducible, and eco-friendly method [17, 44] that allows the preparation of high catalysts amount in a single step. During the ball milling process, kinetic energy from moving balls is transferred to the powders, resulting in small particle sizes, high surface areas, and active sites that ultimately increase photocatalytic activity [45].

In the present study, anatase-rutile TiO_2 was synthesized with a high specific surface area and then coupled with different percentages of Cu_2O, through a simple and eco-friendly ball milling method, in order to broaden the absorption of light towards the visible, improve charge transfer processes and increase H_2 production. Photoreforming of different sacrificial agents, such as formic acid, ethanol, glucose and glycerol, was performed to generate H_2 in a pilot plant photo-reactor under natural sunlight irradiation. Mechanistic studies were conducted to identify the main active species affecting the photocatalysts' performance. Future efforts will be focused on improving the catalyst optimized here to obtain performing samples to be used in pilot-scale

117 reactors not only for H_2 production but also for the synthesis of high-value-added compounds and
118 CO_2 reduction.

119 2. Results and discussions

120 2.1 Characterizations

121 Figure 1A shows the UV-Vis DRS spectra of the samples used. Cu_2O displays absorbance only in
122 the visible range, while HP TiO_2 powder shows a transition edge at ca. 340 nm and a significant
123 light absorption in the range 400-650 nm, ascribable to the presence of oxygen vacancies as can
124 be inferred from the spectrum shape in accordance with the literature [46, 47]. In the composite
125 samples, a gradual increase in absorbance at wavelengths higher than 400 nm and a second
126 absorption edge associated with Cu_2O can be noticed by increasing Cu_2O from 1 to 5%. The band
127 gap of home prepared TiO_2 is 3.03 eV (Table 1), that of Cu_2O 1.97 eV, and in the composites the
128 addition of Cu_2O to TiO_2 does not alter the band gap, but two transitions can be noticed. The one
129 at lower wavelength is coincident with that of the hosted oxide, the second one is ascribable to
130 Cu_2O. The presence of the two edges suggests the formation of a heterostructure between the two
131 oxides [17, 48]. In Table 1 the SSA values of the samples used are reported. The surface area of
132 bare TiO_2 is 78 $m^2 g^{-1}$, that of Cu_2O 1 $m^2 g^{-1}$ and its addition to TiO_2 causes only a small decrease
133 in SSA due to the low Cu_2O amount and mild preparation conditions of the heterostructures.
134 In Figure 1B the photoluminescence spectra of selected samples are shown. The photocatalysts
135 exhibit two main emission peaks: the one at ca. 420 nm comes from the band-to-band emission
136 caused by the recombination of photogenerated charges, while the peaks at higher wavelengths
137 can be attributed to the recombination of photo-promoted electrons into defects due to oxygen
138 vacancies [49]. The coupling of TiO_2 with 3% and 5% Cu_2O causes a reduction in the

photoluminescence intensity due to a decrease in the recombination rate of photogenerated charges [50] while no significant changes can be observed for 1%Cu_2O. This result can probably be explained by simply considering that the amount of hosted oxide is lower. Notably, the 3%Cu_2O-TiO_2 sample exhibits the lowest intensity indicating an optimal charge transfer rate that can be associated with a high photocatalytic activity.

The different conduction energy levels and valence band edges for TiO_2 and Cu_2O led to interfacial charge transfer, decreasing the e^-/h^+ recombination rate.

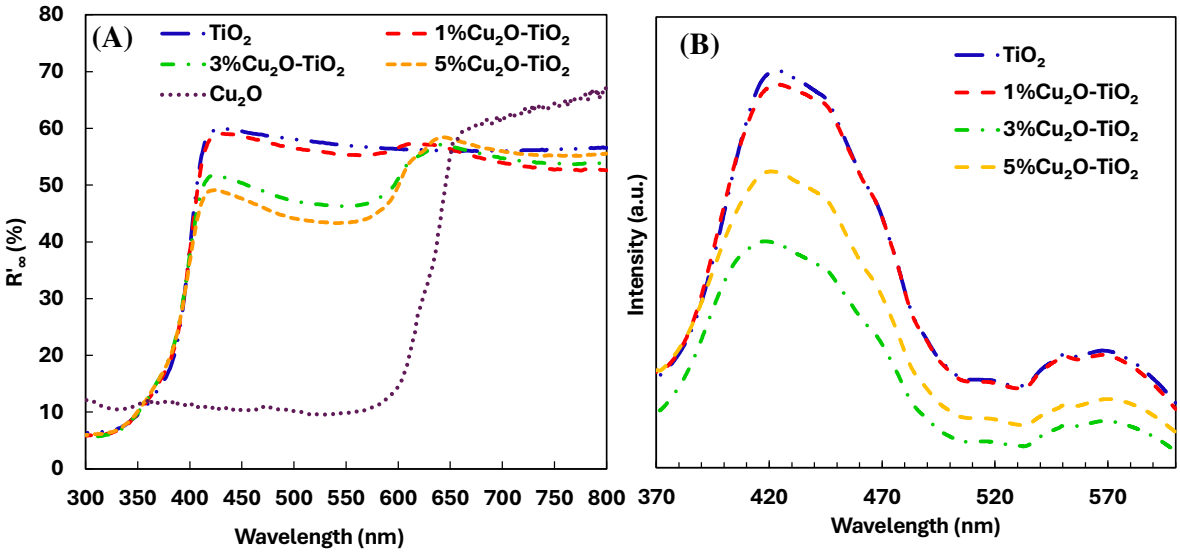

Figure 1. UV-Vis DRS spectra of the used samples (A); photoluminescence spectra of TiO_2 HP and 3%Cu_2O-TiO_2 HP samples (B).

Table 1. Band gap and SSA values of the used photocatalysts.

Samples	Band gap (eV)	SSA ($m^2 \cdot g^{-1}$)

TiO_2 HP	3.03	78
1%Cu_2O-TiO_2 HP	3.02	72
3%Cu_2O-TiO_2 HP	3.02	69
5%Cu_2O-TiO_2 HP	3.03	68
Cu_2O	1.97	1

152

153 Figure 2A reports the XRD diffractograms of the TiO_2 HP and 3% Cu_2O-TiO_2 HP samples. The
154 first sample consists of a mixture of anatase (main peak at $2\theta = 25.28°$) and rutile (main peak at
155 $2\theta = 27.53°$) phases. After the addition of Cu_2O, two peaks at $2\theta = 36.5°$ and 42.4° were also
156 recorded, corresponding to the (111) and (200) crystal planes of Cu_2O, respectively, in agreement
157 with the literature [51].
158 The relative amount of anatase and rutile, contained in the crystalline part of TiO_2, was determined
159 by the following equations [52]:

160 $$W_A = \frac{0.886 \cdot A_A}{0.886 \cdot A_A + A_R}$$

161 $$W_R = \frac{A_R}{0.886 \cdot A_A + A_R}$$

162 In which A_A and A_R represent the integrated intensity of the anatase peak at $2\theta = 25.3°$ and of the
163 rutile one at $2\theta = 27.5°$, respectively. Bare TiO_2 HP consisted of ca. 77.5 % of anatase and 22.5%
164 of rutile exhibiting a phase composition very similar to that of TiO_2 P25. After the ball milling
165 treatment in the presence of 3% Cu_2O, the relative amounts of anatase and rutile were 83 and 17%,
166 respectively. An explanation can be found in the fact that, during ball milling, a crystallization of
167 part of the amorphous phase into the anatase phase occurred, and in support of this hypothesis it

should be noted that the peaks in the diffractogram of 3%Cu_2O-TiO_2 HP are narrower and more intense than those of the starting pure TiO_2.

In Figure 2B the Raman spectra of bare TiO_2 HP and its composite with 3% Cu_2O are reported. In the TiO_2 sample, only the characteristic anatase bands at 144 cm^{-1}, 197 cm^{-1}, 396 cm^{-1}, 514 cm^{-1} and 637 cm^{-1} are visible, whilst no band attributable to rutile is present due to its lower content with respect to anatase. In 3%Cu_2O-TiO_2 HP no peaks of Cu_2O are visible, probably due to the low amount and high degree of dispersion on TiO_2 surface. However, by enlarging the main anatase peak associated with the O-Ti-O vibration (inset of Figure 1B), a slight red shift, attributable to a bond distortion into the TiO_2 lattice, can be noticed [53]. This finding confirms an interaction between TiO_2 and Cu_2O in the composite samples.

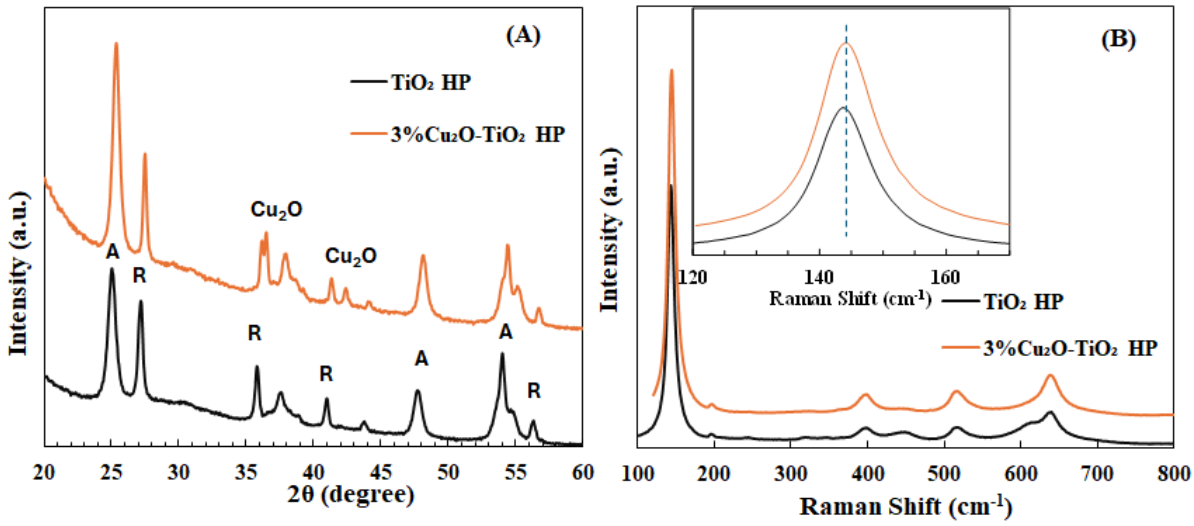

Figure 2. XRD patterns (A) and Raman spectra (B) of TiO_2 HP and 3%Cu_2O-TiO_2 HP.

Figure 3 (A,B) shows the SEM images of TiO_2 HP and 3%Cu_2O-TiO_2 HP powders. Irregular rounded-shaped aggregates with sizes ranging from 20 to 130 nm can be observed in TiO_2 HP, without changes in morphology after the addition of Cu_2O, probably due to the relatively small

184 amount of Cu_2O compared to TiO_2 and uniform mixing. The morphology of the powder recovered
185 after photocatalytic tests (Figure 3C) is substantially the same as that of the "fresh" sample,
186 indicating that the photocatalyst is stable to the mechanical stresses due to mixing in water. TEM
187 images were also acquired to study the distribution of components and particles dimensions. In
188 Figure 3 (D), Cu_2O showed particle size ranges between 5 and 10 nm, while sizes of TiO_2 HP
189 particles were between 5 and 25 nm. The lattice fringes of ca. 0.35 nm can be attributed both to
190 the (101) plane (d= 0.352 nm) of anatase TiO_2 or to the (110) (d= 0.324 nm) of rutile TiO_2 (due to
191 the small difference between the two values and the relative low content of rutile) [54, 55], while
192 the lattice fringes of Cu_2O (200) planes are ca. 0.22 nm [56].

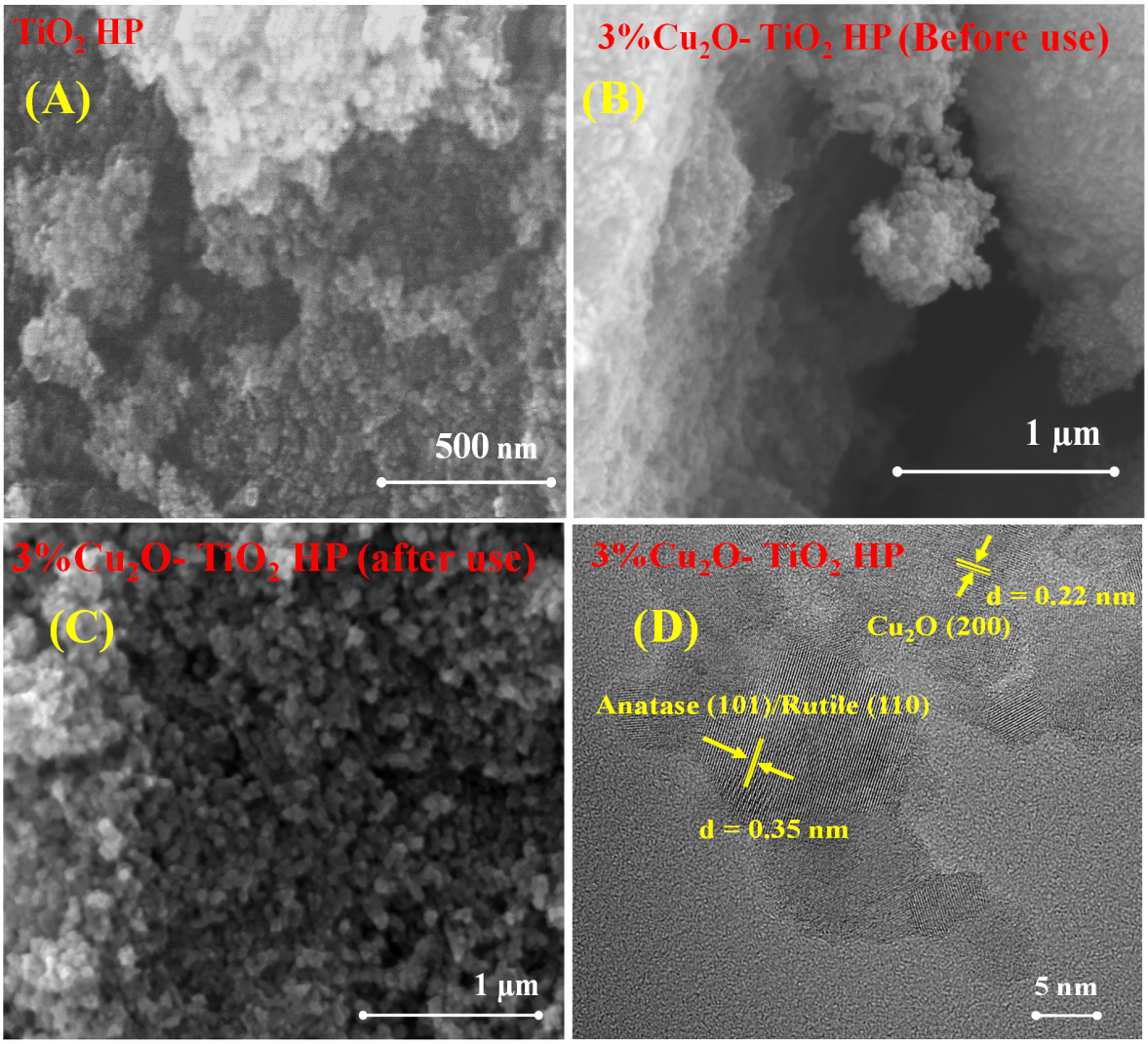

Figure 3. SEM images of TiO_2 HP (A), 3%Cu_2O-TiO_2 HP before (B) and after the photocatalytic tests (C) and TEM image of 3%Cu_2O-TiO_2 HP (D).

Figure 4A shows the XPS binding energy peaks characteristic of Ti 2p, O 1s and Cu 2p species present in bare TiO_2 and in the 3%Cu_2O-TiO_2 samples. Peaks identified in bare TiO_2 at binding energies 459.1 eV and 464.9 eV are representative of Ti 2p3/2 and Ti 2p1/2 transitions, respectively. The presence of these two peaks, with a binding energy separation of 5.8 eV, indicates that Ti is present mainly in the +4 oxidation state [57]. The minor signal at 470 eV (better

visible in the deconvolution of the spectrum (Figure 4B)) is reported as a shake-up satellite band reflecting weak background effects or subtle surface species that does not significantly alter the assignment of Ti^{4+} in TiO_2 [58]. In the 3%Cu_2O-TiO_2 HP composite the Ti 2p peaks display a little shift towards lower binding energies, and this behaviour can be ascribed to the formation of surface Ti^{3+} species, probably due to some degree of oxidation of Cu^+ to Cu^{2+} [59, 60]. For both samples, the O 1s spectra have a main peak at 530.7 eV (see Figures 4) associated with O_2^- ions in the crystal TiO_2 structure, and when also Cu_2O is present additional peaks are present at 532.7 and 535.3 eV, corresponding to hydroxyl groups and water molecules adsorbed on the catalyst surface [61]. The presence of oxygen vacancies enhances the adsorption capacity of the catalysts' surface towards water and hydroxyl radicals, thus increasing the H^+ adsorption and H_2 formation [62, 63]. The spectrum related to Cu 2p shows two main peaks located at 937.2 eV and 957.4 eV characteristic of $2p_{3/2}$ and $2p_{1/2}$ transitions of Cu^+, while the minor peak at 946.2 eV associated with the Cu^{2+} 2p3/2 transition indicates the presence of a little amount of Cu^{2+} ions [47] because of the instability of Cu^+ species. Additionally, the peak near 933 eV (Figure 4B) suggests the presence of Cu^+ or metallic Cu^0, pointing to a mixture of copper oxidation states in the sample. However, as can be seen from the spectra, copper is mainly present as Cu^+ and Cu^{2+}, although further small amounts of Cu^0 could form under irradiation [41]. Moreover, the deconvolution of the spectra (Figure 4B) allowed to clearly separate and distinguish the two peaks relating to O_2^- and OH^-.

Notably, the intensity ratio of the copper peaks Cu $2p_{3/2}$ and Cu $2p_{1/2}$ does not correspond to the ideal value equal about 2:1 because the Cu 2p spectrum is sensitive to the chemical environment of the copper atom [64-66]. In our case, the co-existence of different oxidation states of Cu contributes to altering the intensity ratio.

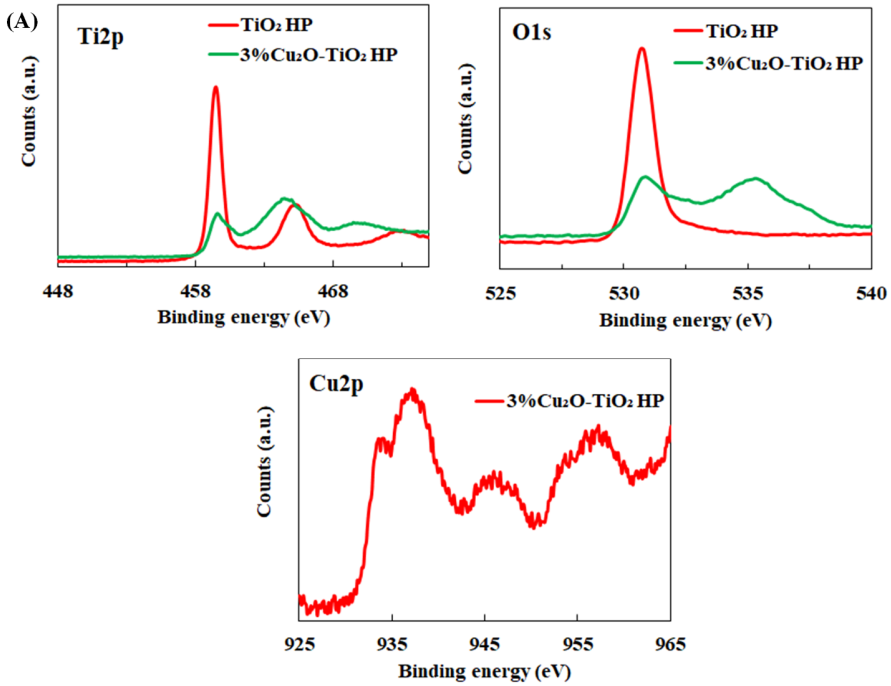
(A)
Ti2p
TiO₂ HP
3%Cu₂O-TiO₂ HP
Counts (a.u.)
448
458
468
Binding energy (eV)
O1s
TiO₂ HP
3%Cu₂O-TiO₂ HP
Counts (a.u.)
525
530
535
540
Binding energy (eV)
Cu2p
3%Cu₂O-TiO₂ HP
Counts (a.u.)
925
935
945
955
965
Binding energy (eV)

223

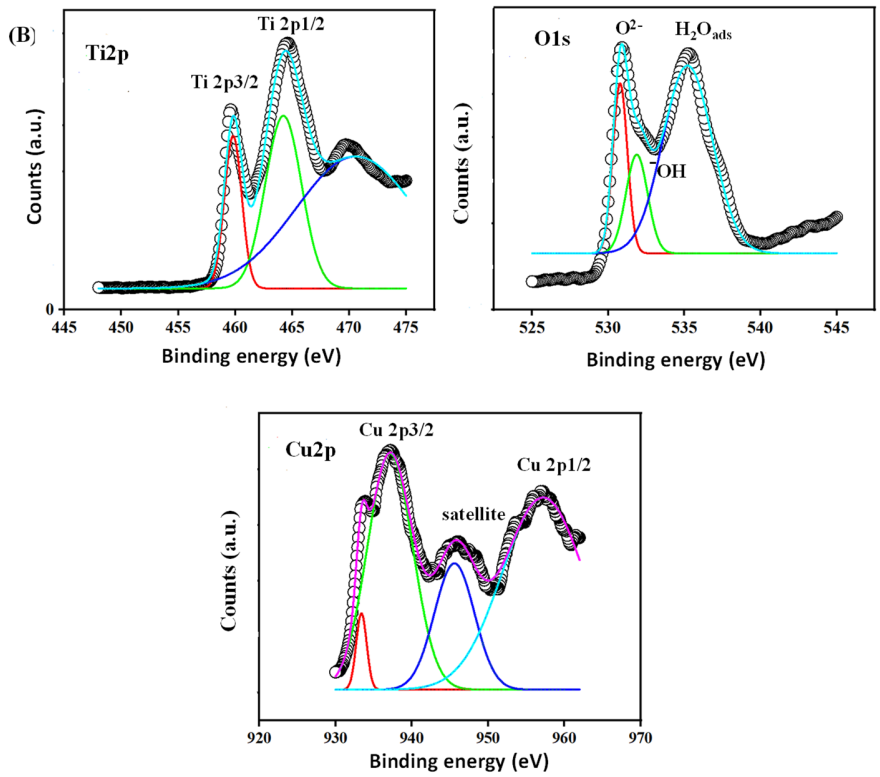
(B)
Ti2p
Ti 2p1/2
Ti 2p3/2
Counts (a.u.)
0
445
450
455
460
465
470
475
Binding energy (eV)
O1s
O²⁻
H₂O ads
OH
Counts (a.u.)
525
530
535
540
545
Binding energy (eV)
Cu2p
Cu 2p3/2
Cu 2p1/2
satellite
Counts (a.u.)
920
930
940
950
960
970
Binding energy (eV)

224

Figure 4. XPS spectra related to Ti 2p, O 1s, and Cu 2p regions (A) and their deconvolution (B) for TiO_2 and 3%Cu_2O-TiO_2 samples.

In Figure 5, the EPR spectra recorded under dark and irradiation for the 3%Cu_2O-TiO_2 photocatalyst are reported. In the presence of DMPO and H_2O_2 (Figure 5A), weak signals related to hydroxyl radicals can be detected both in the absence and the presence of light, underlining the possible formation of a certain amount of $^{\bullet}OH$ radicals. In the solution containing H_2O/DMPO/MeOH (Figure 5B), no EPR signal is present in the absence of light, indicating that the photocatalyst did not generate superoxide anion radicals ($^{\bullet}O_2^-$) in the dark; under irradiation, instead, the characteristic peaks attributed to the paramagnetic resonance peaks of the DMPO-$^{\bullet}O_2^-$ adduct [67, 68] are visible.

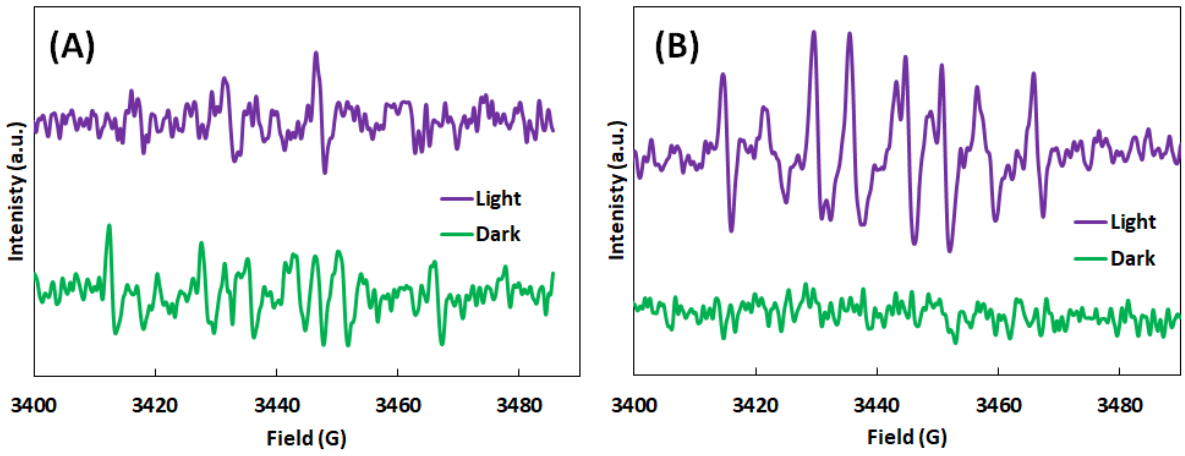

Figure 5. EPR spectra of the 3%Cu_2O-TiO_2 sample under dark and light irradiation: (A) sample dispersed in H_2O/DMPO/H_2O_2 solution, and (B) sample dispersed in H_2O/DMPO/MeOH solution.

Photoelectrochemical measurements were performed to investigate the impact of Cu_2O addition on the electronic properties of TiO_2. The photocurrent spectra, recorded in 0.1 M ABE at the open-circuit potential (80 mV and 120 mV vs. Ag/AgCl for TiO_2 and 3%Cu_2O-TiO_2, respectively), are presented in Figures 6A and B. In particular, while for bare TiO_2 only one peak is present, for 3%Cu_2O-TiO_2, a maximum of the secondary photocurrent appears between 350 nm and 400 nm, indicating the presence of electronic transitions of the two components.

Assuming non-direct optical transitions, the optical band gap (E_g) values of the studied photocatalysts can be determined using Equation (1):

Eqn. 1) $$(Q_{ph}\, h\nu)^{0.5} \propto (h\nu - E_g)$$

where hν is the photon energy, and Q_{ph} represents the photocurrent yield, corrected for the efficiency of the lamp monochromator system. Since this correction is proportional to the light absorption coefficient near the band gap, the optical band gaps are estimated by extrapolating the $(Q_{ph} \cdot h\nu)^{0.5}$ vs. hν plots to zero (Figures 6C and D).

For TiO_2, an E_g of 3.2 eV was determined, whereas for 3%Cu_2O-TiO_2, two band gaps were identified at 3.0 eV, related to TiO_2, and at 2.1 eV attributed to Cu_2O. The presence of photocurrent at photon energies below the TiO_2 band gap suggests optical transitions within Cu_2O, which has a lower band gap than TiO_2 polymorphs.

Figures 6E and F illustrate the effect of light irradiation on the open-circuit potential (OCP) for TiO_2 and 3%Cu_2O-TiO_2 under the same experimental conditions. Upon irradiation, OCP shifts negatively for TiO_2, consistent with n-type semiconductor performance. This behaviour is further confirmed by transient current measurements, where manual interrupting irradiation results in an

anodic photocurrent (Figure 6G). However, for 3%Cu_2O-TiO_2, a less negative photopotential is observed due to the opposing effects of light irradiation on n-type TiO_2 (negative shift) and p-type Cu_2O (positive shift) (Figure 6F). This is in accordance with transient photocurrent data (Figure 6H) recorded for the 3%Cu_2O-TiO_2 sample, which show an initial cathodic photocurrent spike followed by a steady anodic photocurrent. After irradiation, conduction band electrons from Cu_2O initially generate a cathodic photocurrent. However, the interfacial built-in potential directs electrons toward the current collector while holes migrate toward the oxide/electrolyte interface, ultimately generating an anodic photocurrent.

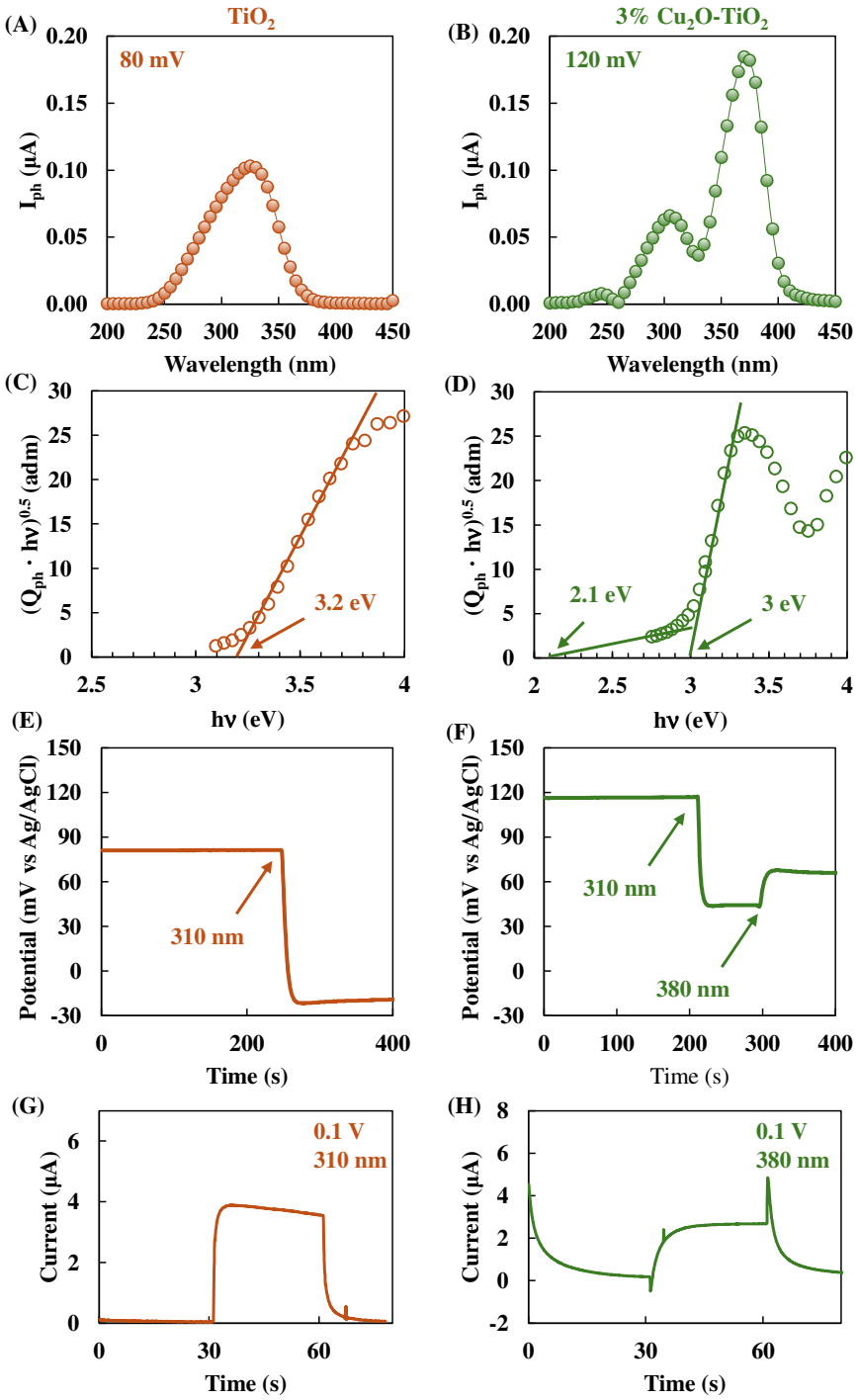

273

274 **Figure 6**. Photocurrent spectra for A) TiO_2, B) 3%Cu_2O-TiO_2, recorded in ABE 0.1 M solution.

275 C) and D) show the respective $(Q_{ph} \cdot h\nu)^{0.5}$ vs hν plots. Photopotential recorded in ABE 0.1 M for

276 TiO_2 and 3%Cu_2O-TiO_2, are reported in E) and F) respectively. G) and H) show the current–time
277 transients recorded for TiO_2 and 3%Cu_2O-TiO_2 respectively.
278

279 ## 2.2 Photocatalytic activity results

280 To evaluate the effect of Cu_2O coupled with TiO_2 HP for H_2 formation, the photoreforming of
281 different sacrificial agents was studied. In particular, formic acid, ethanol, glucose and glycerol
282 were used. The group of sacrificial agents was selected due to their low splitting energy demand
283 of 32.9, 29, 46.7 and 3.9 $kJ \cdot mol^{-1}$ respectively, compared to 237.13 $kJ \cdot mol^{-1}$ for pure water.
284 Furthermore, the appropriate position of their redox potential with respect to the valence band
285 energy of the semiconductor makes them suitable for trapping photogenerated holes capable of
286 oxidizing organic substances.
287 The 3%Cu_2O-TiO_2 HP sample was initially chosen as the photocatalyst only to select the sacrificial
288 agent with which to subsequently conduct the optimization of the amount of Cu_2O in TiO_2 HP,
289 since previous work carried out in lab-scale reactors with commercial TiO_2 instead of TiO_2 HP
290 indicated that the 3% Cu_2O percentage gave the best results [17,69].
291 The use of sacrificial agents such as ethanol and glucose resulted in poor H_2 generation, yielding
292 4.1 mmol (STH, of 0.13%) and 3.4 mmol (STH of 0.11%) respectively, at H_{UV} of 420 $kJ \cdot m^{-2}$, as
293 shown in Figure 7. The highest H_2 amount was obtained adding glycerol and formic acid as
294 sacrificial compounds. In particular, the amount of H_2 generated with formic acid (Figure 7) was
295 33.9 mmol (STH of 1.05%), very similar to that measured with glycerol (STH of 1.07%) at 420
296 $kJ \cdot m^{-2}$. The results obtained are in accordance with literature data. Chen et al. [70] investigated the
297 activity of Au/TiO_2 photocatalysts in alcohols–H_2O mixtures and the H_2 production followed the
298 order: glycerol > ethylene glycol > methanol > ethanol. Bowker [71], meanwhile, found that the

rate decreased in the order glycerol > glucose > methanol > ethanol. Bahruji et al. [72], analyzing the behaviour of 20 different starting compounds, found the following reactivity order: triols > diols > 2° alcohols > 1° alcohols > 3° alcohols and assumed that the sacrificial agent displaying an α-H adjacent to the OH group(s) has a higher H_2 production activity.

Ethanol contains a single α-H adjacent to the hydroxyl group, which provides less reactive sites for oxidation reactions, and glucose, also displaying an α-H adjacent to the OH group, has a complex molecular structure and may require more energy to break down into H_2 and other intermediates before its mineralization. Formic acid has the simplest molecular structure that undergoes simple reactions producing H_2 and CO_2, and the single carboxyl group in its molecule facilitates a highly efficient pathway for electron donation to form H_2. Glycerol containing three hydroxyl groups is easy to oxidize, and provides more reactive sites, resulting in high H_2 generation. Features such as the presence of several hydroxyl groups in the structure, the length of the carbon chain, and dehydrogenation characteristics of sacrificial agents have a direct effect on H_2 generation [73]. Additionally, some other characteristics including polarity, the ability to be adsorbed by the surface of the photocatalyst and the production of byproducts, could have a significant impact on H_2 production efficiency and intermediate products [74, 75]. The obtained results confirmed the effectiveness of Cu_2O in replacing noble metals for H_2 production under solar irradiation and the formation of an efficient Cu_2O/TiO_2 heterostructure.

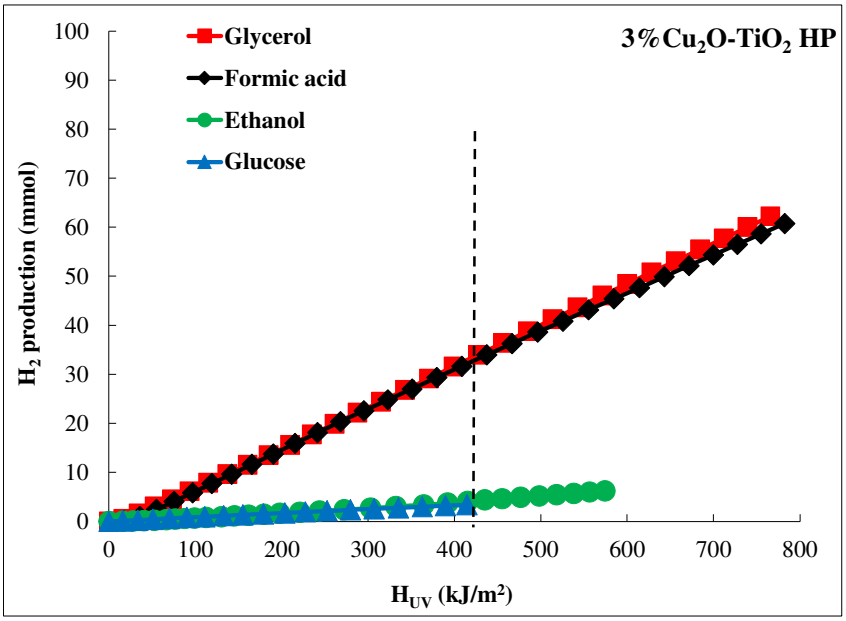

Figure 7. H_2 generation with glycerol, formic acid, ethanol, and glucose in the presence of 3%Cu_2O-TiO_2 HP.

The highest amount of H_2 was produced in the presence of both formic acid and glycerol, but since formic acid is a valuable chemical in the pharmaceutical, chemical, agricultural and textile industries, while glycerol is a waste product, the latter was used as a sacrificial agent to optimize the Cu_2O/TiO_2 HP ratio.

The used concentration of glycerol was 0.075M, as determined in a previous study [76]. In Figure 8, the amount of produced H_2 by using different Cu_2O TiO_2 HP photocatalysts is plotted versus H_{UV}. Results were compared at H_{UV} 660 ± 5 kJ·m^{-2} (value obtained after approximately 4.5 h of irradiation), since it was common to all tests. In the presence of 1%Cu_2O-TiO_2 HP a H_2 evolution of 42.2 mmol (STH of 0.86%) was obtained, suggesting the effectiveness of the Cu_2O-TiO_2 HP heterostructure [17]. The increase of Cu_2O into TiO_2 had a positive effect on H_2 formation, and with the 3%Cu_2O-TiO_2 HP sample was 53.1 mmol (STH of 1.10%), 26% higher than that of 1%Cu_2O-TiO_2 HP. However, by further increasing the amount of Cu_2O in TiO_2, the H_2 production

efficiency decreased, being 48.3 mmol (STH of 0.99%) the H_2 obtained in the presence of the 5% Cu_2O-TiO_2 HP sample, as shown in Figure 8.

It can be stated that at the lowest percentage (1%) there was a lower number of active sites due to the addition of Cu_2O to form the composite, compared to the sample with 3%, while at the highest amount (5%) a higher number of sites on the TiO_2 surface were covered and therefore deactivated since the light could not reach them. The amount of 3% of Cu_2O has proven to be the best among those used favouring the formation of an optimal number of surface-active sites of TiO_2 and Cu_2O, also inducing a good mutual interaction between the two components [72], in accordance with photoluminescence results. An excessive increase of Cu_2O can produce the formation of agglomerates and reduce the effectiveness of the Cu_2O-TiO_2 HP heterojunction, essential for a high photocatalytic production of H_2. Furthermore, the decrease of the absorbed light, due to the TiO_2 covering effect, reduces the ability to generate electron-hole pairs. The low difference in the specific surface area values does not justify the different photoactivity of the various samples.

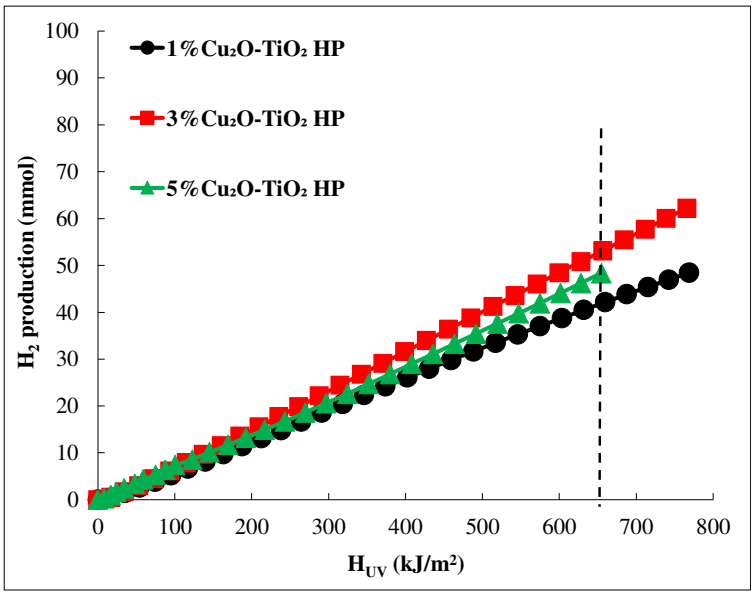

348 **Figure 8.** H_2 generation with 1%Cu_2O-TiO_2 HP, 3%Cu_2O-TiO_2 HP, and 5%Cu_2O-TiO_2 HP
349 (Glycerol 0.075 M, 100 mg·L^{-1} photocatalyst).

350 The formation of H_2 in the presence of Cu_2O-TiO_2 HP photocatalysts can be explained by
351 assuming a charge transfer between the components (Figure 9) [47]. When two different
352 polymorphs of TiO_2 are present, the surface phase junction between them enables an effective
353 electron transfer between the particles, which results in an efficient charge separation. Particularly,
354 the CB edge of anatase being more negative than that of rutile, electrons, after irradiation, will
355 transfer from the former to the second phase and, due to the slightly more positive value of the VB
356 edge of anatase with respect to rutile, holes will be transferred from anatase to the VB of rutile.
357 Furthermore, when a p-type semiconductor is in contact with an n-type semiconductor, an internal
358 electric field will be formed at the interface, which will generate a movement of charges according
359 to a type-II heterojunction [77]. In addition, under irradiation, photoexcited e^-/h^+ pairs are produced
360 in both Cu_2O and TiO_2. Considering the energy band levels of rutile and Cu_2O, holes will transfer
361 from the VB of TiO_2 to the VB of Cu_2O and electrons from the CB of Cu_2O to the CB of TiO_2.
362 The holes accumulated in the VB of Cu_2O will oxidize sacrificial agents producing organic
363 intermediates, CO_2 and H^+ ions and the electrons collected in the rutile TiO_2 CB will reduce H^+ to
364 H_2. These charge transfers significantly reduce the recombination of photogenerated charges as
365 indicated by PL results, thus increasing the photocatalytic capacity of the composites for H_2
366 production.

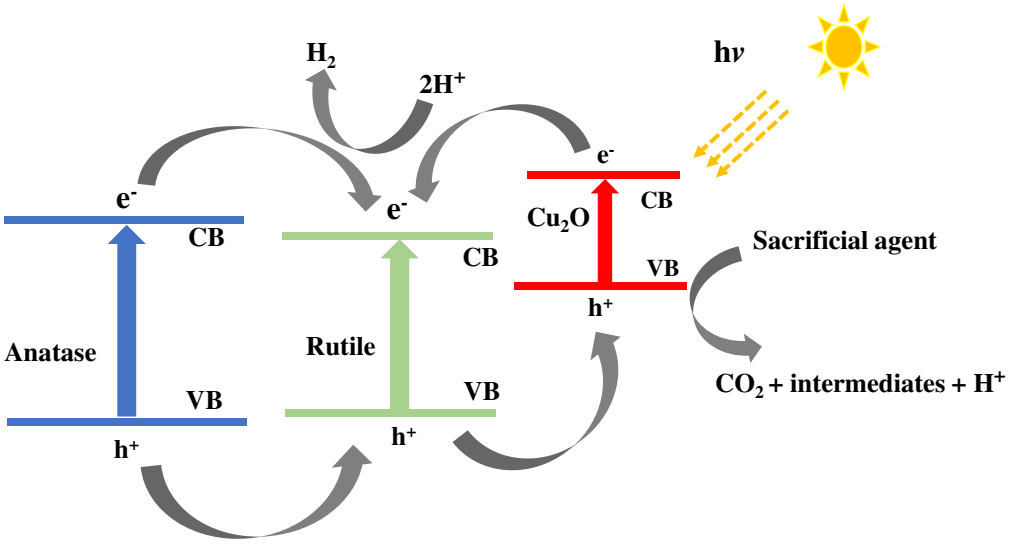

367

368 **Figure 9.** Proposed reaction mechanism for H_2 generation in the presence of Cu_2O-TiO_2 HP.

369 Notably, the color of CPC tubes under irradiation was turned into garnet-purple, this could be due
370 to the formation of some amount of Ti^{3+} species (blue colored) attributed to the transfer of electrons
371 from Cu^{+} to Ti^{4+} (as reported in the XPS results description) with the formation of Cu^{2+} species
372 and/or the formation of some amounts of Cu^{0}, in accordance with the literature [39]. Both species
373 can play a positive role on photoactivity as Ti^{3+} creating electronic states below the conduction
374 band responsible for visible light absorption, while Cu^{0} takes part to redox processes, enhancing
375 the charges transfer process [78, 79].
376 This is also in accordance with the scheme reported in Figure 9, which justifies the transfer of
377 holes from TiO_2 to Cu_2O. The garnet-purple color of the reaction mixture could be due to a mixture
378 of light blue (Ti^{3+}) and red (Cu_2O) and/or to the presence of Cu^{0}. A study on the occurrence and
379 extent of possible copper leaching is reported below.
380 During photoreforming, the formation of short-chain carboxylic acids (Figure 10) was followed
381 by ionic chromatography. Figure 10A shows the evolution of formic acid (FA) during the
382 photoreforming of glycerol. It was the main product, but probably other compounds formed in

383 traces, such as glycolic acid (GA), were not detected as below the quantification limit of the
384 analytical protocol. However, it can also be assumed that other reaction products were probably
385 rapidly converted into formic acid. The partial oxidation of the initial substrate was faster than the
386 mineralization of formic acid, and therefore this acid was able to accumulate in the water.
387 The highest formic acid amount was observed with 3%Cu_2O-TiO_2 HP, which also gave the highest
388 H_2 production. This result can be explained by considering that a greater use of holes for the
389 glycerol oxidation reaction corresponds to a greater availability of electrons for the reduction of
390 H^+, confirming the fundamental role of sacrificial agents for the production of H_2.
391 FA was also the main measured intermediate product (before mineralization) deriving from
392 glucose (Figure 10B); in the presence of ethanol, only small quantities of FA were observed, in
393 agreement with the low production of H_2. Traces of GA and acetic acid were also detected but not
394 reported for the sake of brevity.
395

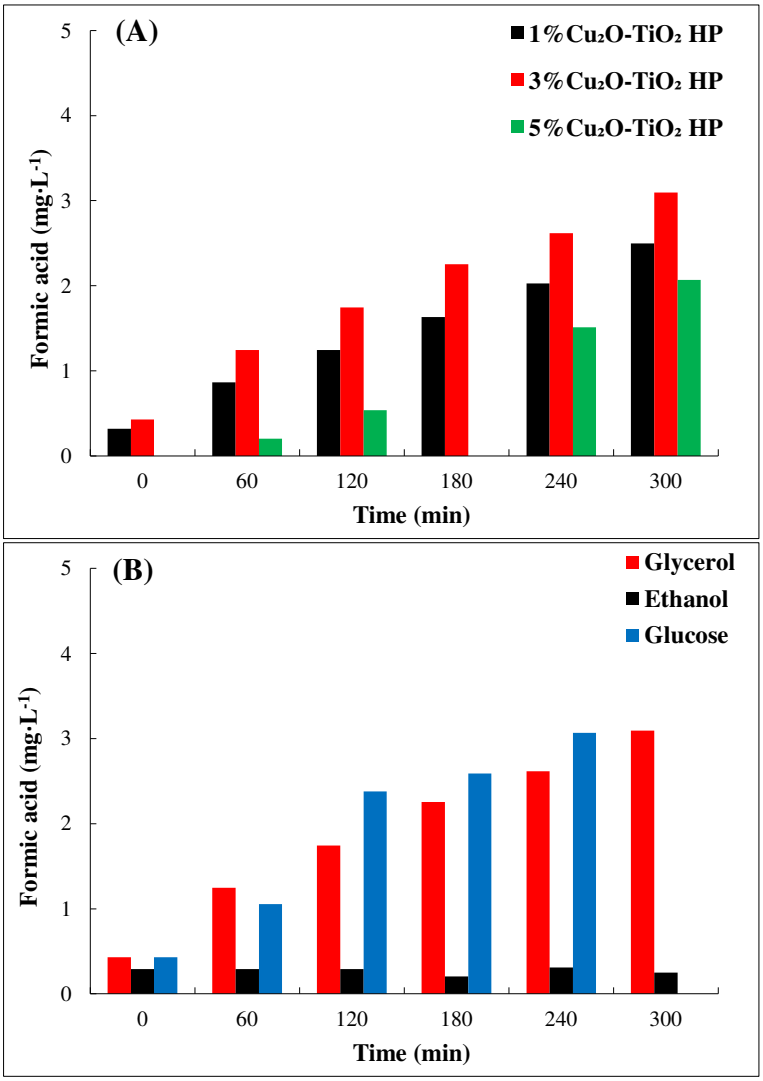

396

397 **Figure 10.** (A) Formation of formic acid (FA) with different photocatalysts in the presence of
398 glycerol as a sacrificial agent. (B) Formation of FA with glycerol, ethanol and glucose as sacrificial
399 agents in the presence 3%Cu_2O-TiO_2 HP.

400 During the experiments, except when formic acid was used as sacrificial agent, a decrease in pH
401 from ~7.5 to ~4.5 was observed. When formic acid was used as sacrificial agent, since the decrease
402 in pH with the other sacrificial agents was due to the formation of short-chain carboxylic acids,
403 the pH remained almost unchanged at the initial value provided by formic acid (pH ~ 3.3). The

404 temperature of the reaction system increased significantly during the tests, i.e. from ~29 °C to ~52
405 °C, but this did not cause any significant change in the rate of H_2 formation (Figures 7 and 8), as
406 is usual in heterogeneous photocatalysis and discussed in the literature [74].
407 In Figure 11A the results obtained during the glycerol photoreforming in the absence and in the
408 presence of scavengers as tert-butanol (for hydroxyl radicals), $Na_2C_2O_4$ (for holes), $AgNO_3$ (for
409 electrons) and benzoquinone (for superoxide ions) using 3%Cu_2O-TiO_2 HP as photocatalyst under
410 simulated solar light irradiation are reported. Notably, the formation of the superoxide radical can
411 be attributed to the small amount of residual oxygen adsorbed onto the photocatalyst surface.
412 While in the presence of tert-butanol, sodium oxalate and benzoquinone a lower conversion of
413 glycerol is observed, after the addition of silver nitrate an increase in photoactivity is measured.
414 These results suggest that the removal from the reaction mixture of $OH^{\bullet}$ radicals, h^+ and $O_2^{\bullet-}$
415 radicals was detrimental as all species intervene in the glycerol oxidation process, but the holes
416 and superoxide radicals play the predominant role, in accordance with EPR spectra.
417 On the contrary, in the presence of $AgNO_3$, an increase in conversion is observed, which highlights
418 how the removal of electrons makes more holes available for the oxidation process. The respective
419 amounts of H_2 and CO_2 obtained (Figure 11B) confirm these results.
420 Namely, following the addition of tert-butanol and $Na_2C_2O_4$, the production of H_2 and CO_2 was
421 lower than that obtained in the absence of scavengers. No H_2 was obtained, and a higher amount
422 of CO_2 was formed when electrons and superoxide anions were removed. The higher degree of
423 mineralization, therefore, can be attributed to the higher availability of holes after the removal of
424 e^- and $O_2^{\bullet-}$ by the scavengers, $AgNO_3$ and benzoquinone, respectively.

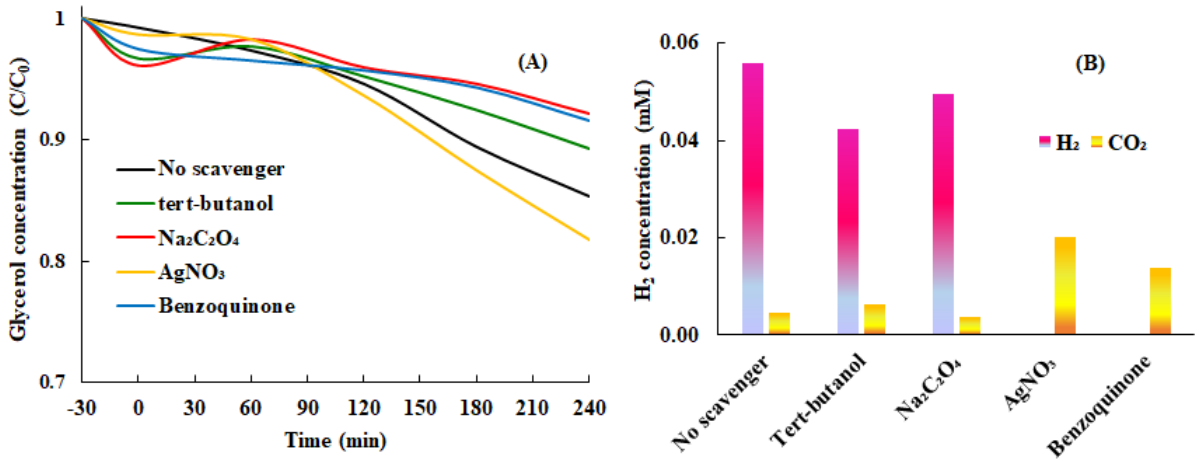

425

426 **Figure 11.** Glycerol concentration versus irradiation time (A) and H_2 and CO_2 amount after 4h of

427 irradiation (B) by using 3%Cu_2O-TiO_2 HP with and without scavenging species.

428

429 ## 2.3 Cu leaching

430 It is important to study the possible leaching of metals from photocatalysts during the

431 photocatalytic reaction. During photoreforming, the formation of organic acids (and subsequent

432 progressive decrease in the pH) could support the dissolution of Cu oxides causing photo-corrosion

433 [80]. Cu leaching was studied by ICP-MS under the best experimental conditions, i.e, with

434 3%Cu_2O-TiO_2 HP and glycerol. During the irradiation, the Cu content in the solution increased

435 and the leaching before the irradiation and after 5 hours of reaction was 0.32 and 2.16 $mg \cdot L^{-1}$,

436 respectively (notably, this value must be evaluated considering that 2.5 g of catalyst are used for

437 each test). To further investigate this aspect, the elementary composition of the sample 3%Cu_2O-

438 TiO_2 HP was examined by an electron microprobe working in an energy dispersive mode (EDX)

439 before and after the photocatalytic runs. The atomic Cu amount on the "fresh" 3%Cu_2O-TiO_2 HP

440 was 1.35 wt%, very close to the nominal one (1.2 wt %) while after the recovery at the end of the

441 run, the amount drops to 0.93% confirming the occurrence of a small copper leak.

Cu leaching is a negative issue; however, this work can be considered as an initial study demonstrating the efficacy of a simple and eco-friendly ball milling method to prepare photocatalytic systems containing semiconductors more stable than Cu_2O for H_2 production on a pilot scale in noble metal free conditions. Various approaches, such doping, surface passivation and other modification methods, can be explored to fine-tune the surface properties of Cu_2O, improving its photocorrosion resistance and thus increasing its stability.

An in-depth study of the various technologies is necessary to evaluate the pros and cons of the different approaches. Passivation, for example, consists in coating a material so that it becomes "passive", that is, less readily corroded by the environment. However, passivation involves the formation of an outer layer of shield material that can decrease the photoactivity by covering the active sites of the catalyst.

3. Conclusions

Coupling Cu_2O with home-prepared TiO_2 was successful for solar-to-hydrogen (STH) conversion in a pilot plant photoreactor. The TiO_2/Cu_2O composites showed an enhanced response in visible-light region and good activity for H_2 production [66]. The formation of p-n heterojunction, as confirmed by electrochemical measures, promotes charges separation, the formation of oxygen vacancies and increased water adsorption capability which result in a good photocatalytic activity. The produced H_2 followed the order: glycerol ≈ formic acid > ethanol ≈ glucose and 62 mmol were obtained after 5h of natural sun-light irradiation (corresponding to an H_2 evolution rate of ca. 5 mmol $g^{-1}h^{-1}$) by using glycerol as sacrificial agent. Mechanistic investigation carried out in a lab-scale reactor by following the glycerol reforming in the presence of selected scavengers confirmed that h^+, $OH^\bullet$ and $O_2^{\bullet-}$ radicals are active species for glycerol degradation whilst electrons have the

leading role in the reduction of H^+ ions to H_2. Although a slight leaching of Cu species has been observed after the photocatalytic runs, however the facile preparation of composite photocatalysts active for solar H_2 production without the use of noble metals deserves to be further explored. Future studies, moreover, should be addressed to increase the stability of the photocatalyst to eliminate any leaching effect.

Acknowledgment

CIEMAT – Plataforma Solar de Almería wish to thank the Grant PLEC2021-007906 (SolFuture) funded by MCIN/AEI/ 10.13039/501100011033 and, by "NextGenerationEU"/PRTR" for partial financing of this study. The Authors thank Prof. Giovanni Palmisano (Khalifa University, Abu Dhabi, UAE) for TEM, XPS and EPR measurements and Dr. Caludio Maria Pecoraro (University of Palermo) for electrochemical characterizations.

References

[1] P.J. Megía, A.J. Vizcaíno, J.A. Calles, A. Carrero, Hydrogen production technologies: From fossil fuels toward renewable sources. A mini review. Energy Fuels. 35 (20) (2014) 16403–16415. https://doi.org/10.1021/acs.energyfuels.1c02501

[2] F. Dawood, M. Anda, G.M. Shafiullah, Hydrogen production for energy: An overview. *Int. J. Hydrogen Energy*. 45 (7) (2020) 3847–3869. https://doi.org/10.1016/j.ijhydene.2019.12.059

[3] T. Ishaq, M. Yousaf, I.A. Bhatti, A. Batool, M.A. Asghar, M. Mohsin, M. Ahmad, A perspective on possible amendments in semiconductors for enhanced photocatalytic hydrogen generation by water splitting. *Int. J. Hydrogen Energy*. 46 (79) (2021) 39036–39057. https://doi.org/10.1016/j.ijhydene.2021.09.165

[4] European Commission, Communication from the Commission to the European Parliament, the European Council, the Council, the European Economic and Social Committee and the Committee of the Regions: The European Green Deal. *European Commission*, Brussels, 2019. https://eur-lex.europa.eu/legal-content/EN/TXT/?uri=CELEX%3A52019DC0640

[5] D. Lei, L. Wang, Y. Lv, N. Luo, Z. Wang, Engineering applications of solar photocatalysis and photothermal catalysis for hydrogen production from biomass: A review. *Chem. Eur. J.* (2024) e202401486. https://doi.org/10.1002/chem.202401486

[6] P. Afanasev, A. Askarova, T. Alekhina, E. Popov, S. Markovic, A. Mukhametdinova, A. Cheremisin, E. Mukhina, An overview of hydrogen production methods: Focus on hydrocarbon feedstock. *Int. J. Hydrogen Energy*. 78 (2024) 805–828. https://doi.org/10.1016/j.ijhydene.2024.06.369

[7] G. Xie, K. Zhang, B. Guo, Q. Liu, L. Fang, J.R. Gong, Graphene-based materials for hydrogen generation from light-driven water splitting. *Adv. Mater.* 25 (28) (2013) 3820–3839. https://doi.org/10.1002/adma.201301207

[8] T. Montini, M. Monai, A. Beltram, I. Romero-Ocaña, P. Fornasiero, H_2 production by photocatalytic reforming of oxygenated compounds using TiO_2-based materials. *Mater. Sci. Semicond. Process.* 42 (1) (2016) 122–130. https://doi.org/10.1016/j.mssp.2015.06.069

[9] K. Shimura, H. Yoshida, Heterogeneous photocatalytic hydrogen production from water and biomass derivatives. *Energy Environ. Sci.* 4 (7) (2011) 2467–2481. https://doi.org/10.1039/c1ee01120k

[10] W. Rulkens, Sewage sludge as a biomass resource for the production of energy: Overview and assessment of the various options. *Energy Fuels*. 22 (1) (2008) 9–15. https://doi.org/10.1021/ef700267m

[11] P. Liu, Z. Cai, Y. You, H. Huang, S. Chen, C. Gao, Z. Qi, et al., Surface modification on Pd–TiO_2 hybrid nanostructures towards highly efficient H_2 production from catalytic formic acid decomposition. *Chem. Eur. J.* 24 (69) (2018) 18398–18402. https://doi.org/10.1002/chem.201803267

[12] Z. Zhang, S.-W. Cao, Y. Liao, C. Xue, Selective photocatalytic decomposition of formic acid over AuPd nanoparticle-decorated TiO_2 nanofibers toward high-yield hydrogen

519 production. *Appl. Catal. B Environ.* 162 (2015) 204–209.
520 https://doi.org/10.1016/j.apcatb.2014.06.055
521 [13] M. Umair, G. Palmisano, R. Al Sakkaf, S. Al Jitan, A. Pintar, G. Žerjav, et al., Pt–Nb_2O_5–
522 TiO_2 based semiconductors for photo-reforming of glucose and fructose aqueous solutions.
523 *Appl. Surf. Sci.* 648 (2024) 159030. https://doi.org/10.1016/j.apsusc.2023.159030
524 [14] L. Da Vià, C. Recchi, E.O. Gonzalez-Yañez, T.E. Davies, J.A. Lopez-Sanchez, Visible
525 light selective photocatalytic conversion of glucose by TiO_2. *Appl. Catal. B Environ.* 202
526 (2017) 281–288. https://doi.org/10.1016/j.apcatb.2016.08.035
527 [15] X. Luo, X. Ge, S. Cui, Y. Li, Value-added processing of crude glycerol into chemicals and
528 polymers. *Bioresour. Technol.* 215 (2016) 144–154.
529 https://doi.org/10.1016/j.biortech.2016.03.042
530 [16] C.R. Coronado, J.A. Carvalho, C.A. Quispe, C.R. Sotomonte, Ecological efficiency in
531 glycerol combustion. *Appl. Therm. Eng.* 63 (2014) 97–104.
532 https://doi.org/10.1016/j.applthermaleng.2013.11.004
533 [17] C.M. Pecoraro, M. Bellardita, V. Loddo, F. Di Franco, L. Palmisano, M. Santamaria, A
534 facile way to synthesize noble metal free TiO_2-based catalysts for glycerol photoreforming.
535 *J. Ind. Eng. Chem.* 118 (2023) 247–258. https://doi.org/10.1016/j.jiec.2022.11.010
536 [18] V. Maurino, A. Bedini, M. Minella, F. Rubertelli, E. Pelizzetti, C. Minero, Glycerol
537 transformation through photocatalysis: A possible route to value-added chemicals. *J. Adv.*
538 *Oxid. Technol.* 11 (2008) 184–192. https://doi.org/10.1515/jaots-2008-0201
539 [19] A. Fujishima, T.N. Rao, D.A. Tryk, Titanium dioxide photocatalysis. *J. Photochem.*
540 *Photobiol. C* 1 (2000) 1–21. https://doi.org/10.1016/S1389-5567(00)00002-2
541 [20] A. Fujishima, K. Honda, Electrochemical photolysis of water at a semiconductor electrode.
542 *Nature* 238 (1972) 37–38. https://doi.org/10.1038/238037a0
543 [21] J.A. Rengifo-Herrera, C. Pulgarin, Why five decades of massive research on heterogeneous
544 photocatalysis, especially on TiO_2, has not yet driven to water disinfection and
545 detoxification applications? Critical review of drawbacks and challenges. *Chem. Eng. J.*
546 477 (2023) 146875. https://doi.org/10.1016/j.cej.2023.146875
547 [22] Y. Cai, Y.P. Feng, Review on charge transfer and chemical activity of TiO_2: Mechanism
548 and applications. *Prog. Surf. Sci.* 91 (2016) 183–202.
549 https://doi.org/10.1016/j.progsurf.2016.11.001

[23] M. Humayun, F. Raziq, A. Khan, W. Luo, Modification strategies of TiO_2 for potential applications in photocatalysis: A critical review. *Green Chem. Lett. Rev.* 11 (2018) 86–102. https://doi.org/10.1080/17518253.2018.1440324

[24] J. Chen, F. Qiu, W. Xu, S. Cao, H. Zhu, Recent progress in enhancing photocatalytic efficiency of TiO_2-based materials. *Appl. Catal. A Gen.* 495 (2015) 131–140. https://doi.org/10.1016/j.apcata.2015.02.013

[25] A.R. Aguirre, A.C. Reina, J.P. Pérez, G. Colon, S. Malato, Catalysts and photoreactors for photocatalytic solar hydrogen production: Fundamentals and recent developments at pilot scale. In: *Photocatalytic Hydrogen Production for Sustainable Energy*, Wiley, 2023, pp. 275–303. https://doi.org/10.1002/9783527835423.ch12

[26] V. Kumaravel, S. Mathew, J. Bartlett, S.C. Pillai, Photocatalytic hydrogen production using metal-doped TiO_2: A review of recent advances. *Appl. Catal. B Environ.* 244 (2019) 1021–1064. https://doi.org/10.1016/j.apcatb.2018.11.080

[27] M. Bellardita, E.I. García-López, G. Marcì, L. Palmisano, Photocatalytic formation of H_2 and value-added chemicals in aqueous glucose (Pt)-TiO_2 suspension. *Int. J. Hydrogen Energy* 41 (2016) 5934–5947. https://doi.org/10.1016/j.ijhydene.2016.02.103

[28] J. Low, J. Yu, M. Jaroniec, S. Wageh, A.A. Al-Ghamdi, Heterojunction photocatalysts. *Adv. Mater.* 29 (2017) 1601694. https://doi.org/10.1002/adma.201601694

[29] S. Meng, W. Sun, S. Zhang, X. Zheng, X. Fu, S. Chen, Insight into the transfer mechanism of photogenerated carriers for WO_3/TiO_2 heterojunction photocatalysts: Is it the transfer of band–band or Z-scheme? Why? *J. Phys. Chem. C* 122 (2018) 26326–26336. https://doi.org/10.1021/acs.jpcc.8b07524

[30] J. Feng, M. Cui, H. Liu, F. Zhou, S. Bi, D. Zhang, Design of an efficient photocatalyst: A type II heterojunction for enhanced hydrogen production driven by visible light. *Phys. Chem. Chem. Phys.* 23 (2021) 11893–11899. https://doi.org/10.1039/D1CP00347J

[31] Y.-H. Zhang, M.-M. Liu, J.-L. Chen, K.-F. Xie, S.-M. Fang, Dendritic branching Z-scheme Cu_2O/TiO_2 heterostructure photocatalysts for boosting H_2 production. J. Phys. Chem. Solids. 152 (2021) 109948. https://doi.org/10.1016/j.jpcs.2021.109948

[32] M. Rafique, S. Hajra, M. Irshad, M. Usman, M. Imran, M.A. Assiri, et al., Hydrogen production using TiO_2-based photocatalysts: A comprehensive review. ACS Omega. 8 (2023) 25640–25648. https://doi.org/10.1021/acsomega.3c00963

[33] A. Di Paola, M. Bellardita, R. Ceccato, L. Palmisano, F. Parrino, Highly active photocatalytic TiO_2 powders obtained by thermohydrolysis of TiCl4 in water. J. Phys. Chem. C. 113 (2009) 15166–15174. https://doi.org/10.1021/jp904673e

[34] T. Ohno, K. Sarukawa, M. Matsumura, Photocatalytic activities of pure rutile particles isolated from TiO_2 powder by dissolving the anatase component in HF solution. J. Phys. Chem. B. 105 (2001) 2417–2420. https://doi.org/10.1021/jp003211z

[35] R.I. Bickley, T. Gonzalez-Carreno, J.S. Lees, L. Palmisano, R.J. Tilley, A structural investigation of titanium dioxide photocatalysts. J. Solid State Chem. 92 (1991) 178–190. https://doi.org/10.1016/0022-4596(91)90255-G

[36] X. Jiang, M. Manawan, T. Feng, R. Qian, T. Zhao, G. Zhou, et al., Anatase and rutile in Evonik Aeroxide P25: Heterojunctioned or individual nanoparticles? Catal. Today. 300 (2018) 12–17. https://doi.org/10.1016/j.cattod.2017.06.010

[37] D.C. Hurum, A.G. Agrios, K.A. Gray, T. Rajh, M.C. Thurnauer, Explaining the enhanced photocatalytic activity of Degussa P25 mixed-phase TiO_2 using EPR. J. Phys. Chem. B. 107 (2003) 4545–4549. https://doi.org/10.1021/jp0273934

[38] F. Parrino, M. Bellardita, E.I. García-López, G. Marcì, V. Loddo, L. Palmisano, Heterogeneous photocatalysis for selective formation of high-value-added molecules: Some chemical and engineering aspects. ACS Catal. 8 (2018) 11191–11225. https://doi.org/10.1021/acscatal.8b03093

[39] F. Plascencia-Hernández, E. Albiter, G.M. Nawfal, C. Colbeau-Justin, H. Remita, H. Pfeiffer, M.A. Valenzuela, Unraveling the effect of low Cu_2O loading on P25 TiO_2 and its self-reduction during methanol photoreforming. Inorg. Chem. Commun. 158 (2023) 111541. https://doi.org/10.1016/j.inoche.2023.111541

[40] E. do Couto-Pessanha, V. M. Paiva, M. D. R. Henriques, A. C. Rodrigues, F. E. Almeida, A. Berger, L. H. da Silva, M. J. Izumi, H. V. Fajardo, TiO_2/Cu_2O heterojunction with ultrafine Cu_2O dispersion and enhanced performance for solar-driven hydrogen production: A low-temperature, ambient pressure, and common stabilizing agent-free synthesis approach, *ACS Omega* 10 (2025) 39814–39822. https://doi.org/10.1021/acsomega.5c03805

[41] S. Rajendran, S.S. Mani, T.R. Nivedhitha, A.K. Asoka, P.S. Arun, T. Mathew, C.S. Gopinath, Facile one-pot synthesis of $CuxO/TiO_2$ photocatalysts by regulating Cu

612 oxidation state for efficient solar H_2 production. ACS Appl. Energy Mater. 7 (2023) 104–
613 116. https://doi.org/10.1021/acsaem.3c02272
614 [42] M.O. Segovia-Guzmán, M. Román-Aguirre, J.Y. Verde-Gomez, V.H. Collins-Martínez,
615 G. Zaragoza-Galán, V.H. Ramos-Sánchez, Green Cu_2O/TiO_2 heterojunction for glycerol
616 photoreforming. Catal. Today. 349 (2020) 88–97.
617 https://doi.org/10.1016/j.cattod.2018.05.031
618 [43] J.-L. Chen, S.-Y. Xie, L.-J. Yue, F.-L. Gong, Y.-H. Zhang, Facile synthesis of Cu_2O/TiO_2
619 (P25) composites with enhanced photocatalytic H_2 evolution activity. J. Mater. Sci. Mater.
620 Electron. 32 (2021) 18900–18911. https://doi.org/10.1007/s10854-021-06407-2
621 [44] A.M. Djaballah, M. Bellardita, L. Palmisano, V. Loddo, M. Umair, C.M. Pecoraro, et al.,
622 Facile preparation of $CuBi_2O_4/TiO_2$ hetero-systems employed for simulated solar-light
623 selective oxidation of 4-methoxybenzyl alcohol model compound. Mol. Catal. 546 (2023)
624 113251. https://doi.org/10.1016/j.mcat.2023.113251
625 [45] A. Nigussie, H.C.A. Murthy, A. Bedassa, A review on synthesis, characterization and
626 photocatalytic applications of copper oxide nanostructures. Res. J. Chem. Environ. 25
627 (2021) 6.
628 [46] Q. Zhu, Y. Peng, L. Lin, C.-M. Fan, G.Q. Gao, R.-X. Wang, A.-W. Xu, Stable blue TiO_{2-x}
629 nanoparticles for efficient visible light photocatalysts. J. Mater. Chem. A. 2 (2014) 4429–
630 4437. https://doi.org/10.1039/C3TA14484D
631 [47] J. L. Chen, M.-M. Liu, S.-Y. Xie, L.-J. Yue, F.-L. Gong, K.-M. Chai, Y.-H. Zhang, Cu_2O-
632 loaded TiO_2 heterojunction composites for enhanced photocatalytic H_2 production. J. Mol.
633 Struct. 1247 (2022) 131294. https://doi.org/10.1016/j.molstruc.2021.131294
634 [48] S. Obregón Alfaro, G. Colón Ibáñez, A ternary Er3+-BiVO4/TiO_2 complex heterostructure
635 with excellent photocatalytic performance. RSC Adv. 4 (2014) 6920–6926.
636 https://doi.org/10.1039/C3RA46603E
637 [49] N.D. Abazović, M.I. Čomor, M.D. Dramićanin, D.J. Jovanović, S.P. Ahrenkiel, J.M.
638 Nedeljković, Photoluminescence of anatase and rutile TiO_2 particles. J. Phys. Chem. B.
639 110 (2006) 25366–25370. https://doi.org/10.1021/jp064454f
640 [50] D. Zhang, Synergetic effects of Cu_2O photocatalyst with titania and enhanced photoactivity
641 under visible irradiation. Acta Chim. Slov. 6 (2013) 141–149. https://doi.org/10.2478/acs-
642 2013-0022

643 [51] M. Kouti, L. Matouri, Fabrication of nanosized cuprous oxide using Fehling's solution.
644 Scientia Iranica. 17 (2010) 73–78. Available from:
645 https://api.semanticscholar.org/CorpusID:54534478
646 [52] H.Z. Zhang, J.F. Banfield, Understanding polymorphic phase transformation behavior
647 during growth of nanocrystalline aggregates: Insights from TiO_2. J. Phys. Chem. B. 104
648 (2000) 3481–3487. https://doi.org/10.1021/jp000499j
649 [53] R. Fiorenza, M. Bellardita, L. D'Urso, G. Compagnini, L. Palmisano, S. Scirè, Au/TiO_2-
650 CeO2 catalysts for photocatalytic water splitting and VOCs oxidation reactions. Catalysts.
651 6 (2016) 121. https://doi.org/10.3390/catal6080121
652 [54] G. Liu, X. Yan, Z. Chen, X. Wang, L. Wang, G.Q. Lu, H.M. Cheng, Synthesis of rutile–
653 anatase core–shell structured TiO_2 for photocatalysis. J. Mater. Chem. 19 (2009) 6590–
654 6596. https://doi.org/10.1039/B902666E
655 [55] L. Miao, P. Jin, K. Kaneko, A. Terai, N. Nabatova-Gabain, S. Tanemura, Preparation and
656 characterization of polycrystalline anatase and rutile TiO_2 thin films by rf magnetron
657 sputtering. Appl. Surf. Sci. 212–213 (2003) 255–263. https://doi.org/10.1016/S0169-
658 4332(03)00106-5
659 [56] D. Zhao, C.M. Tu, X.J. Hu, N. Zhang, Notable in situ surface transformation of Cu_2O
660 nanomaterials leads to dramatic activity enhancement for CO oxidation. RSC Adv. 7
661 (2017) 37596–37603. https://doi.org/10.1039/C7RA05950G
662 [57] A.K.R. Police, S.V.P. Vattikuti, K.K. Mandari, M. Chennaiahgari, M.V. Sharma, D.K.
663 Valluri, C. Byon, Bismuth oxide cocatalyst and copper oxide sensitizer in
664 $Cu_2O/TiO_2/Bi_2O_3$ ternary photocatalyst for efficient hydrogen production under solar light
665 irradiation. Ceram. Int. 44 (2018) 11783–11791.
666 https://doi.org/10.1016/j.ceramint.2018.03.262
667 [58] K.R. Park, D.T. Tran, T.T. Nguyen, N.H. Kim, J.H. Lee, Copper-incorporated
668 heterostructures of amorphous NiSex/crystalline NiSe2 as an efficient electrocatalyst for
669 overall water splitting. Chem. Eng. J. 422 (2021) 130048.
670 https://doi.org/10.1016/j.cej.2021.130048
671 [59] T. Wei, Y.N. Zhu, X.Q. An, L.M. Liu, X.Z. Cao, H.J. Liu, J.H. Qu, Defect modulation of
672 Z-scheme TiO_2/Cu_2O photocatalysts for durable water splitting. ACS Catal. 9 (2019)
673 8346–8354. https://doi.org/10.1021/acscatal.9b01786

[60] X. An, T. Li, B. Wen, J. Tang, Z. Hu, L.M. Liu, J. Qu, C.P. Huang, H. Liu, New insights into defect-mediated heterostructures for photoelectrochemical water splitting. Adv. Energy Mater. 6 (2016) 1502268. https://doi.org/10.1002/aenm.201502268

[61] A. Wiatrowski, M. Mazur, A. Obstarczyk, D. Wojcieszak, D. Kaczmarek, J. Morgiel, D. Gibson, Comparison of the physicochemical properties of TiO_2 thin films obtained by magnetron sputtering with continuous and pulsed gas flow. Coatings. 8 (2018) 412. https://doi.org/10.3390/coatings8110412

[62] C.M. Pecoraro, L. Mino, E. Kozyr, L. Palmisano, F. di Franco, V. Loddo, M. Santamaria, M. Bellardita, Pt–TiO_2 catalysts for glycerol photoreforming: Comparison of anatase, brookite and rutile polymorphs. Chem. Commun. 60 (2024) 3782–3785. https://doi.org/10.1039/D4CC00353E

[63] H. Qian, B. Yuan, Y. Liu, R. Zhu, W. Luan, C. Zhang, Oxygen vacancy enhanced photocatalytic activity of Cu_2O/TiO_2 heterojunction. iScience. 27 (2024) 109578. https://doi.org/10.1016/j.isci.2024.109578

[64] D. Cosma, A. Urda, T. Radu, M.C. Rosu, M. Mihet, C. Socaci, Evaluation of the photocatalytic properties of copper oxides/graphene/TiO_2 nanoparticles composites. Molecules. 27 (2022) 5803. https://doi.org/10.3390/molecules27185803

[65] P. Wang, Z. Liu, C. Han, et al., Cu_2O/CuO heterojunction formed by thermal oxidation and decorated with Pt co-catalyst as an efficient photocathode for photoelectrochemical water splitting. J. Nanopart. Res. 23 (2021) 268. https://doi.org/10.1007/s11051-021-05383-2

[66] F.A. Akgul, G. Akgul, N. Yildirim, H.E. Unalan, R. Turan, Influence of thermal annealing on microstructural, morphological, optical properties and surface electronic structure of copper oxide thin films. Mater. Chem. Phys. 147 (2014) 987–995. https://doi.org/10.1016/j.matchemphys.2014.06.047

[67] W. He, Y. Liu, W.G. Wamer, J.-J. Yin, Electron spin resonance spectroscopy for the study of nanomaterial-mediated generation of reactive oxygen species. J. Food Drug Anal. 22 (2014) 49–63. https://doi.org/10.1016/j.jfda.2014.01.004

[68] J. Qiu, L. Zhang, D. Dai, G. Xia, J. Yao, Cellulose-derived carbon dot-guided growth of ZnIn2S4 nanosheets for photocatalytic oxidation of 5-hydroxymethylfurfural into 2,5-diformylfuran. ChemSusChem. 15 (2022) e202200399. https://doi.org/10.1002/cssc.202200399

[69] M. Muscetta, S. Al Jitan, G. Palmisano, R. Andreozzi, R. Marotta, S. Cimino, I. Di Somma, Visible light–driven photocatalytic hydrogen production using Cu_2O/TiO_2 composites prepared by facile mechanochemical synthesis. J. Environ. Chem. Eng. 10 (2022) 107735. https://doi.org/10.1016/j.jece.2022.107735

[70] W.T. Chen, A. Chan, Z.H.N. Al-Azri, A.G. Dosado, M.A. Nadeem, D. Sun-Waterhouse, H. Idriss, G.I.N. Waterhouse, Effect of TiO_2 polymorph and alcohol sacrificial agent on the activity of Au/TiO_2 photocatalysts for H_2 production in alcohol–water mixtures. J. Catal. 329 (2015) 499–513. https://doi.org/10.1016/j.jcat.2015.06.014

[71] M. Bowker, Photocatalytic hydrogen production and oxygenate photoreforming. Catal. Lett. 142 (2012) 923–929. https://doi.org/10.1007/s10562-012-0875-4

[72] H. Bahruji, M. Bowker, P.R. Davies, F. Pedrono, New insights into the mechanism of photocatalytic reforming on Pd/TiO_2. Appl. Catal. B. 107 (2011) 205–209. https://doi.org/10.1016/j.apcatb.2011.07.015

[73] V. Kumaravel, M.D. Imam, A. Badreldin, R.K. Chava, J.Y. Do, M. Kang, A. Abdel-Wahab, Photocatalytic hydrogen production: Role of sacrificial reagents on the activity of oxide, carbon, and sulfide catalysts. Catalysts. 9 (2019) 276. https://doi.org/10.3390/catal9030276

[74] F.J. López-Tenllado, J. Hidalgo-Carrillo, V. Montes, A. Marinas, F.J. Urbano, J.M. Marinas, L. Ilieva, T. Tabakova, F. Reid, A comparative study of hydrogen photocatalytic production from glycerol and propan-2-ol on M/TiO_2 systems (M = Au, Pt, Pd). Catal. Today. 280 (2017) 58–64. https://doi.org/10.1016/j.cattod.2016.05.009

[75] O. Quiroz-Cardoso, S. Oros-Ruiz, A. Solís-Gómez, R. López, R. Gómez, Enhanced photocatalytic hydrogen production by CdS nanofibers modified with graphene oxide and nickel nanoparticles under visible light. Fuel. 237 (2019) 227–235. https://doi.org/10.1016/j.fuel.2018.10.013

[76] A. Ruiz-Aguirre, J.G. Villachica-Llamosas, M.I. Polo-López, A. Cabrera-Reina, G. Colón, J. Peral, S. Malato, Assessment of pilot-plant scale solar photocatalytic hydrogen generation with multiple approaches: Valorization, water decontamination and disinfection. Energy. 260 (2022) 125199. https://doi.org/10.1016/j.energy.2022.125199

[77] H. Wang, L. Zhang, Z. Chen, J. Hu, S. Li, Z. Wang, J. Liu, X. Wang, Semiconductor heterojunction photocatalysts: Design, construction, and photocatalytic performances. Chem. Soc. Rev. 43 (2014) 5234–5244. https://doi.org/10.1039/C4CS00126E

[78] N. Serpone, Is the band gap of pristine TiO_2 narrowed by anion- and cation-doping of titanium dioxide in second-generation photocatalysts? J. Phys. Chem. B. 110 (2006) 24287–24293. https://doi.org/10.1021/jp065659r

[79] Q. Zhu, Y. Peng, L. Lin, C.-M. Fan, G.-Q. Gao, R.-X. Wang, A.-W. Xu, Stable blue TiO_{2-x} nanoparticles for efficient visible light photocatalysts. J. Mater. Chem. A. 2 (2014) 4429–4437. https://doi.org/10.1039/C3TA14484D

[80] T. Montini, V. Gombac, L. Sordelli, J.J. Delgado, X. Chen, G. Adami, P. Fornasiero, Nanostructured Cu/TiO_2 photocatalysts for H_2 production from ethanol and glycerol aqueous solutions. ChemCatChem. 3 (2011) 574–577. https://doi.org/10.1002/cctc.201000289